Upconversion particle as a local luminescent Brownian probe - a photonic force microscopy study

Flavio M. Mor,* Andrzej Sienkiewicz, László Forró, and Sylvia Jeney

Laboratoire de Physique de la Matière Complexe, Ecole Polytechnique Fédérale de Lausanne (EPFL), CH-1015 Lausanne, Switzerland

E-mail: flavio.mor@epfl.ch

Phone: +41 (21) 693 4438. Fax: +41 (21) 693 4470

SUPPORTING INFORMATION

List of Figures

Instrument

The near-infrared (NIR) beam was expanded (EXP, beam expander, Sill Optics, Germany) for best trapping efficiency and attenuated if necessary by a first neutral density filter (NF1,

*To whom correspondence should be addressed

OWIS, Germany). A polarizing beamsplitter cube (PBS, PBS25-1064-HP, Thorlabs, USA) fixed the laser polarization. A laser line filter (FL, FL1064-3-ø1, Thorlabs, USA) was used to cancel the wavelength of the laser pump. The NIR light was then reflected by a first dichroic mirror (DM1, AHF Analysentechnik AG, Germany) into the high numerical aperture (NA = 1.2) of a 60x water-immersion objective (OBJ, UPLapo/IR, Olympus, Japan), which focused the laser down to its diffraction limit into the object plane of the microscope and creates the optical trap. To avoid saturation of the quadrant photodetector (QPD, G6849, Hamamatsu Photonics, Japan), neutral density filters (NF2, OWIS, Germany) could be placed in front of the QPD, especially when maximal laser powers were used for strong trapping. Two diaphragms (D1 and D2, OWIS, Germany) were used to align the NIR laser (Figure S1, red light).

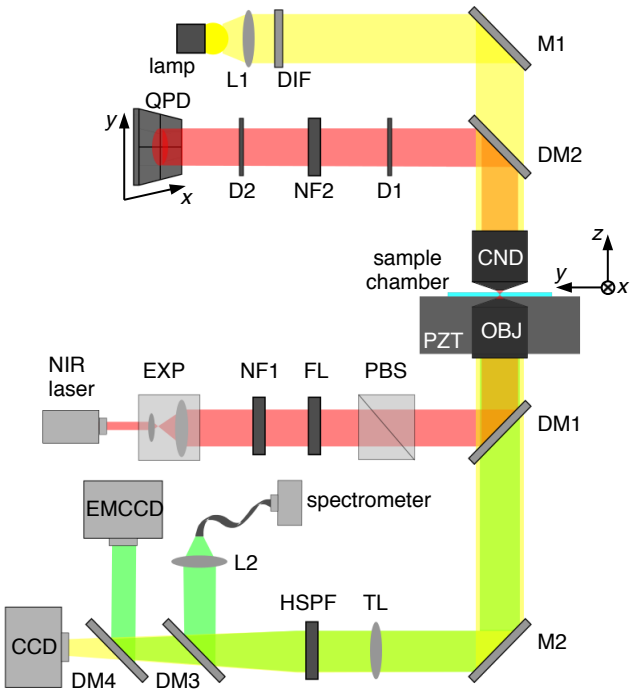

Figure S1: Schematic layout of the NIR (red), visible (yellow) and luminescent (green) light paths.

The sample was mounted onto a piezo scanning stage (PZT, P-561, Physik Instrumente, Germany) for three-dimensional (3D) sample manipulation and positioning, relative to the fixed optical trapping focus. The PZT with controller (E-710.3CD Digital PZT Controller,

Physik Instrumente, Germany) has a travel range of 100 µm along all 3D with a precision of ~ 1 nm. Such a precision was achieved through an electronic feedback system (Figure S1).

For illumination in the visible, the light from a 50-W halogen lamp (OWIS, Germany) was collected by a first lens (L1, Thorlabs, USA), diffused by a diffuser (DIF, OWIS, Germany), then projected by a first mirror (M1, OWIS, Germany) through a condenser objective (CND, 63x, Achroplan, NA = 0.9, water-immersion, Zeiss, Germany), reflected by a second mirror (M2, OWIS, Germany) and focused by a 300-mm tube lens (TL, Thorlabs, USA) onto a charge-coupled device (CCD, ORCA ER S5107, Hamamatsu Photonics, Japan). The PZT, CCD camera, and data acquisition, as well as data analysis and representation were controlled and coordinated by a custom-made software.

The luminescent light emitted by the trapped particle and collected by the OBJ was transmitted by DM1 and focused onto a spectrofluorometer (USB2000-FL-450, Ocean Optics Inc., USA) through the TL and a second lens (L2, Thorlabs, USA). A 400-µm diameter optical fiber brought the luminescent photons to the photosensitive detector. The spectrofluorometer works in the full visible spectrum (360 nm to 1050 nm) and has a resolution in wavelength of ~ 0.35 nm (Figure S1, green light path).

Two 50% dichroic mirrors (DM3 and DM4, Thorlabs, USA) allowed to simultaneously detect the luminescent light spectrum and its spatial distribution through an electron multiplying charge-coupled device (EMCCD, iXon^{EM}+897, Andor Technology, United Kingdom) camera (Figure S1). The EMCCD camera can be cooled down to -90 °C for best quantum efficiency, which reaches a maximum value of 92.5% at 575 nm.

Unlike the spectrofluorometer, the CCD and EMCCD cameras had to be protected from the backscattered 1064-nm laser beam with a holographic notch filter (HSPF, Kaiser Optical System Inc., USA) . Indeed, the maximum wavelength detectable by the spectrofluorometer is ~ 1053 nm, whereas the CCD and EMCCD cameras are sensitive up to 1100 nm (Figure S1).

Morphologies

Random shape β-$NaYF_4$:Yb,Er particles: we studied the morphological characteristics of commercially available β-$NaYF_4$:Yb,Er particles (referred to as UCP in the following). According to the manufacturer [1] (PTIR550/F, Phosphor Technology), they consist of random shape particles, which reach a median size of $\sim 4\,\mu m$.

To reduce the size of the particles and prevent aggregation, the aqueous UCP solution was sonicated on ice during $\sim 30\,min$ at 10-30% of the maximal power with a 3-mm tip probe (Bandelin electronic). Owing the high density of $NaYF_4$ ($\rho_p = 4.21\,kg\,m^{-3}$ [1]) separation of the particles according to their size could be straightforwardly achieved by sedimentation. After a sedimentation time of $\sim 5\,min$, 100 µL were pipetted at different levels in the solution and the phase containing particles smaller than 2 µm were selected for trapping experiments.

Hexagonal shape β-$NaYF_4$:Yb,Er particles: we also studied commercially available UCPs of highly monodisperse hexagonal shape. According to the manufacturer (Intelligent Solutions Inc., Princenton, NJ 08540, USA), they have edge lengths of $\sim 230\,nm$ and a thickness of $\sim 120\,nm$.

To avoid aggregation of the particles, the aqueous UCP solution was first dispersed with a vortex mixer for $\sim 10\,s$ and then sonicated in a water bath for $\sim 5\,min$. The stock solution was finally diluted 100 times.

Optical trapping of single upconversion luminescent particles

Due to their high density, the UCPs sediment at the bottom surface of the PFM sample chamber, where their thermal fluctuations are drastically reduced. This simplifies visualization of even the smaller particles studied here. After $\sim 5\,min$, the great majority of UCPs

[1] http://www.phosphor-technology.com/

could be found at the bottom surface of the sample chamber. Therefore, to ensure single particle trapping, we first searched for a single particle close to the surface and then lifted it up ~ 50 µm into the solution using the optical trap. By continuously monitoring the UCL spectra and Brownian motion of the UCP, we could detect when a second particle entered the trap, which only rarely occurred, as most particles remained below at the surface.

Laser-induced heating in photonic force microscopy

Laser-induced heating in optical trapping has extensively been discussed by several authors.[2–5] E. J. G. Peterman *et al.*[4] showed experimentally that for polystyrene or silica microspheres in aqueous solutions, heating was primarily due to the absorption of light by the fluid, and therefore less dependent on the particle.

Applying the theoretical model developed by E. J. G. Peterman *et al.*[4] to the experimental conditions used in this work, we expect the temperature increase to be of ~ 2°C at the highest laser power of 94 mW (1064 nm) used here.

Even at a trapping wavelength of 980 nm, for which water absorption is known to be higher, and with a 4 times higher laser power, P. Haro-González *et al.*[5] measured a temperature increase in the solution of maximally 21 K, corresponding to heating of 57 K W^{-1}.

Calibration of the spectrofluorometer

The spectral distribution of a light source can be represented in units of wavelength λ, energy E or frequency ν, which can yield to a completely different appearance of the spectrum.[6] In addition, the wavelength-dependent sensitivity of the spectrofluorometer's photosensitive device and the optical response of the set-up have to be taken into account in order not to bias the recorded spectra. Therefore, we carefully quantified either the rate or power of luminescent photons using the black-body (BB) radiation theory.

The photon energy E can be written as a function of the wavelength λ or the frequency

ν as

$$E = h\nu = \frac{hc}{\lambda}, \tag{1}$$

where h denotes the Planck's constant and c the speed of light in free space. Consequently, the infinitesimal bandwidth $\mathrm{d}E$ is given by

$$\mathrm{d}E = h\mathrm{d}\nu = -hc\lambda^{-2}\mathrm{d}\lambda. \tag{2}$$

As expected, $\mathrm{d}E$ is proportional to $\mathrm{d}\nu$, but not to $\mathrm{d}\lambda$. As our spectrofluorometer measured in units of wavelength, special care had to be taken when a spectral band of the photoluminescence spectrum was integrated to obtain either the rate or the power of the photons. In this respect, the Planck's law describes the radiation of a BB in thermal equilibrium either in terms of wavelength λ, or energy E as

$$M_\lambda = \frac{2\pi c}{\lambda^4}\frac{1}{e^{\frac{hc}{\lambda k_\mathrm{B}T}} - 1}, \tag{3}$$

$$M_E = \frac{2\pi}{c^2h^3}\frac{E^2}{e^{\frac{E}{k_\mathrm{B}T}} - 1}. \tag{4}$$

The two functions M_λ and M_E represent the photon rate emitted by a BB source per surface unit and per photon-wavelength interval, $\mathrm{s^{-1}\,m^{-2}\,m^{-1}}$, or per photon-energy interval, $\mathrm{s^{-1}\,m^{-2}\,J^{-1}}$. Similarly, the power of the recorded photons per surface unit and per photon-energy interval, $\mathrm{W\,m^{-2}\,J^{-1}}$, is obtained from

$$P_E = \frac{2\pi}{c^2h^3}\frac{E^3}{e^{\frac{E}{k_\mathrm{B}T}} - 1} = EM_E. \tag{5}$$

To convert the number of events recorded by the spectrofluorometer, which is calibrated in wavelength only, into a photon count rate or power, we used a reference lamp mimicking the radiation of a BB at $T = 2000\,\mathrm{K}$ (Mikropack, Halogen Light Source, HL 2000). The lamp was then placed at the position of the sample in the PFM set-up and the resulting

spectrum, I_{ref}, was recorded by the spectrofluorometer as a function of λ (Figure S2a). The spectrum does not match the emittance of the BB. The difference originates from the optical responses of the set-up and the spectrofluorometer, which are not constant in wavelength. For example, the strong drop at $\sim 536\,\text{nm}$ (Figure S2a, black line) is the consequence of the 1064-nm HSPF filter (Figure S1). In order to obtain a quantitative photoluminescence spectrum in units of energy, a calibration function, ζ_{M_E}, was defined as the ratio between the BB radiation function, M_E and the reference spectrum of the lamp, I_{ref}, as

$$\zeta_{M_E} = \frac{M_E}{I_{\text{ref}}(E)}, \tag{6}$$

where ζ_{M_E} is expressed in units of $\text{events}^{-1}\,\text{m}^{-2}\,\text{J}^{-1}$. The black line in Figure S2b, highlights the behavior of ζ_{M_E} in units of eV rather than J.

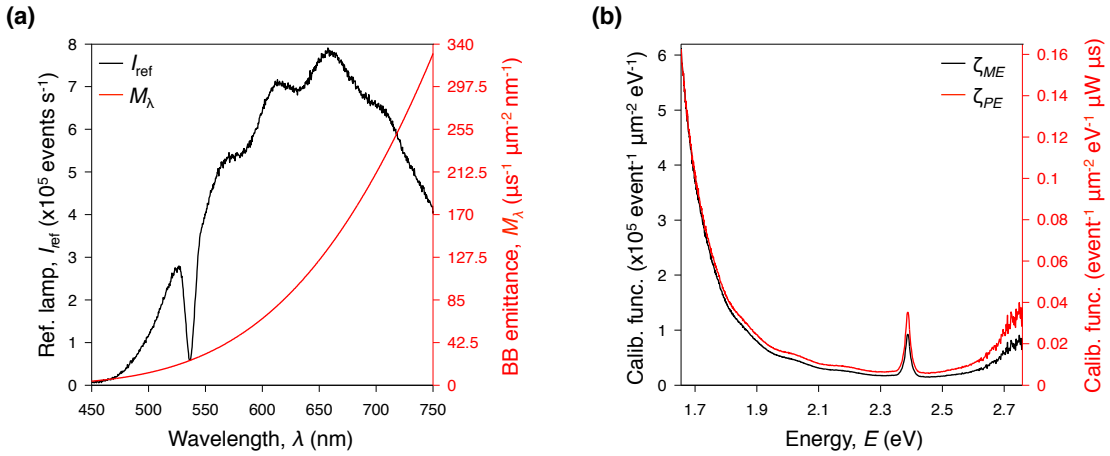

Figure S2: (a) Reference lamp spectrum (black line) recorded by the spectrofluorometer through the experimental set-up as a function of wavelength λ, compared to the expected BB emittance at 2000 K (red line). (b) Resulting calibration functions in units of energy (black line) or power (red line) as a function of energy E. All experimental spectra are recorded during an integration time of $\mathcal{T}_{\text{int}} = 3\,\text{ms}$.

Once ζ_{M_E} was determined, the diameter of the optical fiber, d_{fiber}, bringing the collected luminescent light to the spectrofluorometer and the rectangular width of the entrance slit, w_{slit}, placed just before the detector had to be known in order to render the calibration procedure independent on the surface of detection ($d_{\text{fiber}} = 400\,\mu\text{m}$ and $w_{\text{slit}} = 200\,\mu\text{m}$). The

photoluminescence spectrum calibrated in units of photon rate per photon-energy interval was then given by

$$I_E^{\text{calib}} = d_{\text{fiber}} w_{\text{slit}} \zeta_{M_E} I_{\text{exp}}, \tag{7}$$

with I_{exp} the experimentally measured photoluminescence spectrum, expressed in units of events s^{-1}. Integration of Equation 7 over an energy band yielded the collected photon rate, $\dot{N}_{\text{col}}$, within this band. Similarly, the collected power of the luminescent light between two energy values, E_1 and E_2 could be calculated as

$$P_{\text{col}} = d_{\text{fiber}} w_{\text{slit}} \int_{E_1}^{E_2} \zeta_{P_E} I_{\text{exp}}(E) \mathrm{d}E = d_{\text{fiber}} w_{\text{slit}} \int_{E_1}^{E_2} \frac{P_E}{I_{\text{ref}}(E)} I_{\text{exp}}(E) \mathrm{d}E. \tag{8}$$

The calibration function for power, $\zeta_{P_E} = P_E / I_{\text{ref}}(E)$, is represented by the the red line in Figure S2b. Obviously, the OBJ only collected a fraction of the emitted photoluminescence propagating along the optical axis (Figure S3).

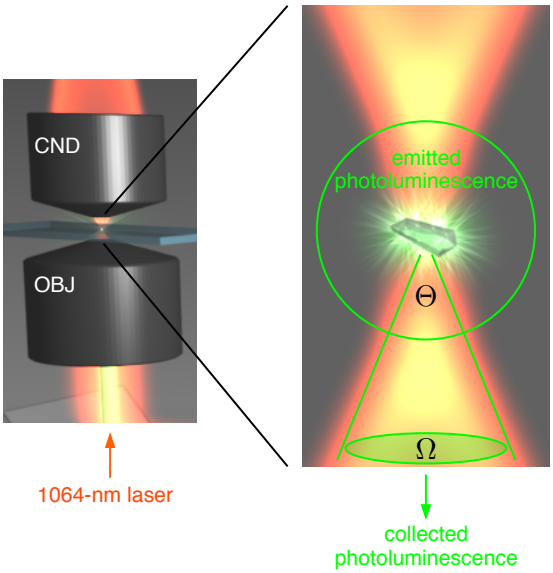

Figure S3: Illustration of the difference between the collected and emitted photoluminescence. Left panel: schematics of the set-up showing the OBJ, which acts as a collector for backward photoluminescence. Right panel: magnification around the trapped luminescent particle highlighting the planar angle Θ and the corresponding solid angle Ω (not drawn to scale) by which the system is observed.

However, in reality, the emission from a trapped UCP radiates over the entire solid angle,

without any preferential direction of propagation. The uncollected photons could be estimated from the cone of the photoluminescent light, which is dependent on the NA of the OBJ through the solid angle $\Omega = 2\pi\,(1 - \cos\,(\Theta/2))$. The planar angle Θ corresponds to the divergence of the light cone. The total solid angle is given when $\Theta = 2\pi$, which leads to $\Omega = 4\pi$. Thereby, the emitted photons rate, $\dot{N}_{\mathrm{emit}}$, and the corresponding power, P_{emit}, could be evaluated assuming a rule of proportionality with the solid angle

$$\frac{4\pi}{\Omega} = \frac{\dot{N}_{\mathrm{emit}}}{\dot{N}_{\mathrm{col}}} = \frac{P_{\mathrm{emit}}}{P_{\mathrm{col}}}, \tag{9}$$

which introduced the correction factor

$$f_{\mathrm{cor}}^{\mathrm{OBJ}} = \frac{4\pi}{\Omega} = \frac{4\pi}{2\pi\,(1 - \cos\,(\Theta/2))} = \frac{2}{1 - \cos\,(\Theta/2)}. \tag{10}$$

According to the definition of the NA[2], we have $\Theta = 2\sin^{-1}(\mathrm{NA}/n_{\mathrm{f}}) = 130.8°$ for NA = 1.2 and $n_{\mathrm{f}} = 1.32$ at 1064 nm. The correction factor is then equal to $f_{\mathrm{cor}}^{\mathrm{OBJ}} = 3.43$. In this estimation, absorption of the fluid surrounding the particle is not taken into account.

The entrance slit placed in front of the spectrofluorometer's photosensitive device cut a part of the photoluminescent photons. Indeed, the diameter of the optical fiber ($d_{\mathrm{fiber}} = 400\ \mu\mathrm{m}$) is larger than the width of the entrance slit ($w_{\mathrm{slit}} = 200\ \mu\mathrm{m}$). In consequence, we had to evaluate another correction factor for the optical fiber as

$$f_{\mathrm{cor}}^{\mathrm{fiber}} = \frac{\pi d_{\mathrm{fiber}}^2/4}{d_{\mathrm{fiber}} w_{\mathrm{slit}}} = \frac{\pi d_{\mathrm{fiber}}}{4 w_{\mathrm{slit}}}, \tag{11}$$

which led to $f_{\mathrm{cor}}^{\mathrm{fiber}} = 1.57$.

[2] http://en.wikipedia.org/wiki/Numerical_aperture

Quantifying the upconversion photoluminescence spectrum

Once the calibration function in terms of power ζ_{P_E} and the correction factor f_{cor} were determined, the experimental UCL spectra, I_{exp}, could be accurately quantified

$$\begin{aligned} I_E^{\mathrm{emit}} &= f_{\mathrm{cor}}^{\mathrm{OBJ}} f_{\mathrm{cor}}^{\mathrm{fiber}} d_{\mathrm{fiber}} w_{\mathrm{slit}} \zeta_{P_E} I_{\mathrm{exp}} \\ &= f_{\mathrm{cor}}^{\mathrm{OBJ}} f_{\mathrm{cor}}^{\mathrm{fiber}} d_{\mathrm{fiber}} w_{\mathrm{slit}} \frac{P_E}{I_{\mathrm{ref}}} I_{\mathrm{exp}}. \end{aligned} \tag{12}$$

A typical example of a UCL spectrum before and after correction is shown in Figure S4. The corrected spectrum has the best S/N between 450 and 750 nm, respectively 2.76 and 1.66 eV. Below $\sim$ 450 nm and above $\sim$ 750 nm, the high noise level of the calibration function ζ_{P_E} distorts the spectrum (Figure S4, black arrows).

The advantage of evaluating spectra expressed in terms of energy E rather than in wavelength λ relies on the fact that E is an extensive physical property, whereas λ is not [3]. Furthermore, The surface under the curve of $I_E^{\mathrm{emit}}(E)$ (Figure S4b), expressed in terms of power, directly yielded the total power of photons emitted by the trapped luminescent particle, which was not the case for $I_E^{\mathrm{emit}}(\lambda)$ (Figure S4a). The corrected UCL shown in Figure S4 has higher photon intensities in the red part ($\sim$ 650 nm) than in the blue ($\sim$ 469 nm) and green ($\sim$ 550 nm) parts of the spectrum. Nevertheless, when looking at a concentrated solution of UCPs excited by a NIR laser, the color of the solution appeared green to a human eye, while the real colors are essentially red and green with a little bit of blue. This is explained by the sensitivity of human color vision, which has a maximum at 555 nm, but it is lower by a factor of $\sim$ 20 at 445 nm and 660 nm [4].

[3] http://en.wikipedia.org/wiki/Intensive_and_extensive_properties
[4] http://en.wikipedia.org/wiki/Color_vision

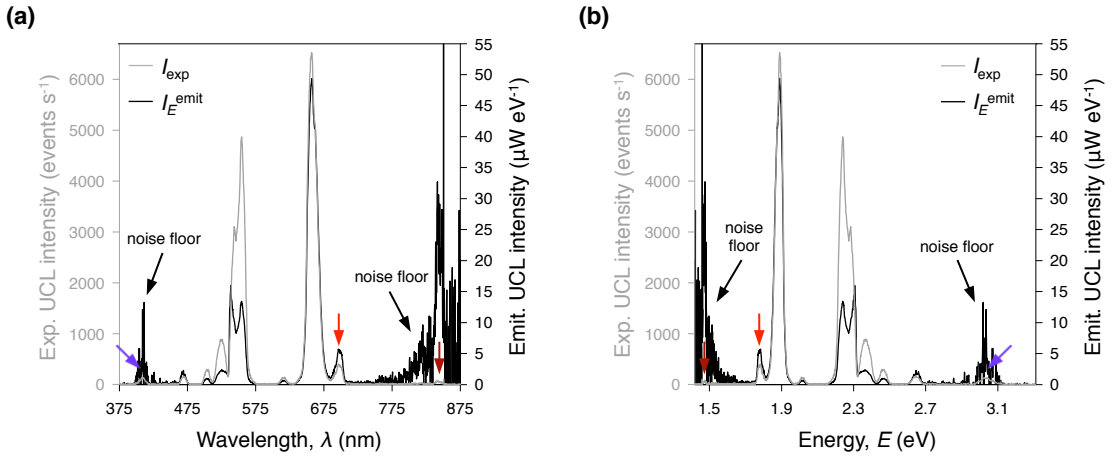

Figure S4: (a) Typical experimental (grey line) and corrected (black line) UCL spectrum as a function of wavelength λ for a single trapped UCP. (b) Corresponding results as a function of energy E. Please note that the color arrows indicates some peaks with different corresponding widths confirming the nonlinear relationship between wavelength and energy.

Test of upconversion photoluminsecence bleaching

According to A. Bednarkiewicz *et al.*[7] and L.H. Fischer *et al.*,[8] the relatively low photobleaching of UCL might originate from small temperature-induced structural changes resulting in deterioration of the hexagonal (β) phase in the core of the particle. Indeed, the temperature at the center of the trapped UCP is higher than in its periphery.[4] Thus, the high laser power density of the strongly focused trapping beam employed in our PFM set-up might lead to a local diminishment of the UCL efficiency, as shown in Figure S5.

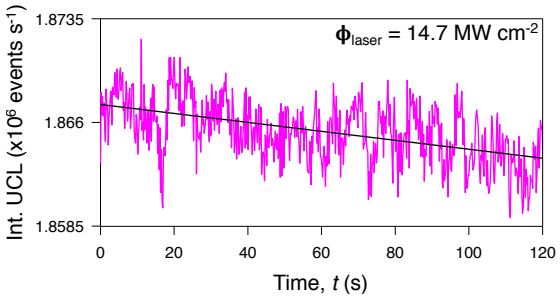

Figure S5: UCL intensity integrated between 450 and 750 nm as a function of time (magenta line) for a typical UCP trapped at maximum laser power density Φ_{laser}. The black line indicates a linear fit, which yields a slope of only ~ 11 events s^{-2} ($\sim 10^{-3}$ % loss).

References

(1) Pyatenko, Y. A.; Voronkov, A. A. The formula of gagarinite. *J. Struct. Chem.* **1962**, *3*, 696–697.

(2) Seol, Y.; Carpenter, A. E.; Perkins, T. T. Gold nanoparticles: enhanced optical trapping and sensitivity coupled with significant heating. *Opt. Lett.* **2006**, *31*, 2429–2431.

(3) Bendix, P. M.; Nader, S.; Reihani, S.; Oddershede, L. B. Direct Measurements of Heating by Electromagnetically Trapped Gold Nanoparticles on Supported Lipid Bilayers. *ACS Nano* **2010**, *4*, 2256–2262.

(4) Peterman, E. J. G.; Gittes, F.; Schmidt, C. F. Laser-Induced Heating in Optical Traps. *Biophys. J.* **2003**, *84*, 1308–1316.

(5) Haro-González, P.; del Rosal, B.; Maestro, L. M.; Rodríguez, E. M.; Naccache, R.; Capobianco, J. A.; Dholakia, K.; Solé, J. G.; Jaque, D. Optical trapping of $NaYF_4$:Er^{3+},Yb^{3+} upconverting fluorescent nanoparticles. *Nanoscale* **2013**, *5*, 12192–12199.

(6) Ejder, E. Methods of Representing Emission, Excitation, and Photoconductivity Spectra. *J. Opt. Soc. Am.* **1969**, *59*, 223–224.

(7) Bednarkiewicz, A.; Wawrzynczyk, D.; Gagor, A.; Kepinski, L.; Kurnatowska, M.; Krajczyk, L.; Nyk, M.; Samooc, M.; Strek, S. Giant enhancement of upconversion in ultrasmall Er^{3+}/Yb^{3+}:$NaYF_4$ nanoparticles via laser annealing. *Nanotechnology* **2012**, *23*, 1–8.

(8) Fischer, L. H.; Harms, G. S.; Wolfbeis, O. S. Upconverting Nanoparticles for Nanoscale Thermometry. *Angew. Chem. Int. Ed.* **2011**, *50*, 4546–4551.